

Hybridized solid-state qubit in the charge-flux regime

J. Q. You,^{1,2} J. S. Tsai,^{1,3} and Franco Nori^{1,4}

¹Frontier Research System, The Institute of Physical and Chemical Research (RIKEN), Wako-shi 351-0198, Japan

²Department of Physics and Surface Physics Laboratory (National Key Laboratory), Fudan University, Shanghai 200433, China

³NEC Fundamental and Environmental Research Laboratories, Tsukuba, Ibaraki 305-8051, Japan

⁴Center for Theoretical Physics, Physics Department, Center for the Study of Complex Systems, University of Michigan, Ann Arbor, MI 48109-1140, USA

(Dated: October 9, 2018)

Most superconducting qubits operate in a regime dominated by either the electrical charge or the magnetic flux. Here we study an intermediate case: a hybridized charge-flux qubit with a third Josephson junction (JJ) added into the SQUID loop of the Cooper-pair box. This additional JJ allows the optimal design of a low-decoherence qubit. Both charge and flux $1/f$ noises are considered. Moreover, we show that an efficient quantum measurement of either the current or the charge can be achieved by using different area sizes for the third JJ.

I. INTRODUCTION

Solid-state qubits based on Josephson-junction (JJ) circuits have attracted considerable attention in recent years and different kinds of Josephson qubits are being explored by taking advantage of the charge and phase (flux) degrees of freedom. Experimentally, quantum oscillations were observed in charge,¹ phase,² and flux qubits.³ A Josephson qubit in the intermediate regime between charge and flux also exhibited quantum oscillations⁴ and showed a high quality factor corresponding to a decoherence time of about $0.5 \mu\text{s}$. Because quantum information processing requires states to evolve coherently in a sufficiently long time, it is thus crucial to obtain qubits with very low decoherence.

Here we study a new type of Josephson qubit, somewhat similar to that in Ref. 4, in which a third JJ is added into the SQUID loop of the Cooper-pair-box (CPB) qubit.¹ In Ref. 4 this third JJ is connected to a current source and only used for measuring the quantum states of the CPB qubit. Moreover, because this JJ is so large, the quantum states of the CPB qubit are only very slightly modified by it. Actually, without a bias current, the large third JJ can be approximated by a harmonic oscillator and the whole system can thus be considered as a CPB qubit coupled to the oscillator. This is very similar to a CPB qubit in a cavity.^{5,6} Very recently, the coherent dynamics of a flux qubit coupled to a harmonic oscillator has been studied,⁷ where the large-size SQUID connected to the qubit plays the role of the harmonic oscillator.

In our present work, the CPB qubit is working in the charge-flux regime, as in Ref. 4, but now the third JJ is *not* necessarily large and more importantly it is *not* used just as a measuring component. This additional degree of freedom in designing the charge-flux qubit allows us to optimize the qubit by changing the size of the third JJ. Indeed, here we show that the charge-flux qubit is gradually *hybridized* (in the quantum mechanical sense) with the third JJ when the area size of this additional JJ decreases. More importantly, we find that the qubit

can be optimized to have the lowest decoherence at a suitable size of the third JJ. Furthermore, we show that efficient quantum measurements of either the current or the charge can be implemented by just choosing different sizes for the third JJ.

The paper is organized as follows. In Sec. II, we present the model Hamiltonian for the hybridized charge-flux qubit and study its properties. Section III shows the energy spectra of the qubit for different sizes of the third junction added into the SQUID loop of the CPB. To analyze the effects of different kinds of noises on the qubit, we employ the boson bath model in which a noise is described by a collection of spectrally distributed harmonic oscillators. The characteristic times for relaxation, decoherence, and leakage of the qubit states are calculated in Sec. IV. We optimize the qubit to have the lowest decoherence by choosing a suitable size for the third junction. Section V is devoted to quantum measurement. We propose two readout schemes to efficiently discriminate qubit states by taking advantage of the charge and flux degrees of freedom. Finally, conclusions are presented in Sec. VI.

II. THE MODEL

The hybridized charge-flux qubit is shown in Fig. 1(a). The third JJ, i.e., the left one, is added into the SQUID loop of the CPB in which an island (denoted by a black dot) is connected by two JJ and coupled to a gate voltage by a capacitance C_g . When $C_1 + C_g = C_2$, the Hamiltonian of the system is given by

$$H = E_{cp}(N - n_g)^2 + E_l(N_3 + \frac{1}{2}n_g)^2 + U, \quad (1)$$

with

$$U = \sum_{i=1}^3 E_{Ji}(1 - \cos \phi_i). \quad (2)$$

Here

$$E_{cp} = 2E_c, \quad E_c = \frac{e^2}{2C_2};$$

$$E_l = \frac{8C_2 E_c}{C_2 + 2C_3}. \quad (3)$$

The phase drops through the three junctions are constrained by

$$\phi_1 - \phi_2 + \phi_3 + 2\pi f_e = 0, \quad (4)$$

where

$$f_e = \frac{\Phi_e}{\Phi_0} \quad (5)$$

is the reduced magnetic flux in the qubit loop (in units of the flux quantum $\Phi_0 = h/2e$). The operator

$$N = -i \frac{\partial}{\partial \phi}, \quad \phi = \frac{1}{2}(\phi_1 + \phi_2),$$

corresponds to the number of Cooper pairs on the island, and

$$N_3 = -i \frac{\partial}{\partial \phi_3}$$

corresponds to the number of Cooper pairs tunneling through the left JJ. Here we consider the simpler case with $E_{J1} = E_{J2} = E_J$, $C_1 = C_2 = C$, $E_{J3} = \alpha E_J$, and $C_3 = \beta C$. In this case, the periodic potential $U(\phi, \phi_3)$ is

$$U = E_J[(2 + \alpha) - 2 \cos \phi \cos(\pi f_e + \frac{1}{2} \phi_3) - \alpha \cos \phi_3], \quad (6)$$

and the condition $C_1 + C_g = C_2$ can be approximately achieved because $C_g \ll C_1, C_2$.

Assuming that the eigenstate of Hamiltonian (1) has the form as follows

$$\Psi(\phi, \phi_3) = e^{in_g(\phi - \frac{1}{2}\phi_3)} \psi(\phi, \phi_3), \quad (7)$$

one can cast the equation for eigenvalues and eigenfunctions

$$H\Psi(\phi, \phi_3) = E\Psi(\phi, \phi_3) \quad (8)$$

to a standard Schrödinger equation with a periodic potential:

$$H_0\psi(\phi, \phi_3) = E\psi(\phi, \phi_3), \quad (9)$$

where

$$H_0 = E_{cp}N^2 + E_pN_3^2 + U(\phi, \phi_3), \quad (10)$$

with $U(\phi, \phi_3)$ given by Eq. (6).

Similar to a flux qubit (see, e.g., Refs. 8 and 9), the reduced Hamiltonian H_0 is just like that for a particle in a two-dimensional periodic potential, so the solution of Eq. (9) has the Bloch-wave form

$$\psi(\phi, \phi_3) = e^{i(k\phi_p + k_3\phi_3)} u_{\mathbf{K}}(\phi, \phi_3), \quad (11)$$

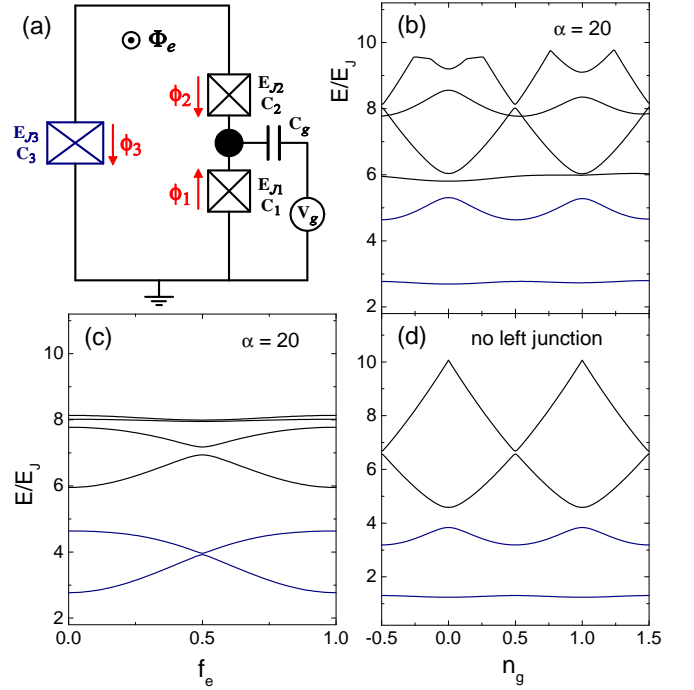


FIG. 1: (Color online) (a) Schematic diagram of the hybridized charge-flux qubit, which consists of three JJs in a superconducting loop (pierced by an external magnetic flux Φ_e) and a superconducting island (denoted by a black dot) coupled to a gate voltage via a capacitance C_g . The Josephson energies and capacitances of the JJs are $E_{J1} = E_{J2} = E_J$, $C_1 = C_2 = C$, $E_{J3} = \alpha E_J$, and $C_3 = \beta C$. Here we consider the charge-flux regime when $E_J = E_c \equiv e^2/2C_2$. Unless explicitly stated otherwise, $\alpha = \beta$ is chosen throughout the paper. Energy levels of the charge-flux qubit versus (b) n_g at $f_e = 0$, and versus (c) f_e at $n_g = 0.5$, where $\alpha = \beta = 20$. (d) Energy levels of the CPB qubit versus n_g at $f_e = 0$, without the left JJ.

where $\mathbf{K} = (k, k_3)$. The constraint

$$(k, k_3) = (-n_g, \frac{1}{2}n_g) \quad (12)$$

on the wave vectors gives rise to

$$\Psi(\phi, \phi_3) = u_{\mathbf{K}}(\phi, \phi_3), \quad (13)$$

which ensures that $\Psi(\phi, \phi_3)$ is periodic in the phases ϕ and ϕ_3 .

Moreover, the Hamiltonian (1) can be rewritten as

$$H = H_{cp} + H_l + H_I, \quad (14)$$

where

$$H_{cp} = E_{cp}(N - n_g)^2 + 2E_J[1 - \cos \phi \cos(\pi f_e)] \quad (15)$$

is the Hamiltonian of a CPB qubit, i.e., the qubit with the left JJ absent in Fig. 1(a), and

$$H_l = E_l(N_3 + \frac{1}{2}n_g)^2 + \alpha E_J(1 - \cos \phi_3) \quad (16)$$

is the effective Hamiltonian of the left JJ. The interaction Hamiltonian

$$H_I = 2E_J \cos \phi \left[\cos(\pi f_e) - \cos\left(\pi f_e - \frac{1}{2}\phi_3\right) \right] \quad (17)$$

represents the coupling between the CPB qubit and the left JJ.

For a large left JJ, the phase drop ϕ_3 is small, so the left JJ can be approximated as a harmonic oscillator with frequency

$$\Omega = \frac{4}{\hbar}(\kappa E_J E_c)^{1/2}, \quad (18)$$

where

$$\kappa = \frac{\alpha}{1 + \beta}. \quad (19)$$

Also, the interaction Hamiltonian can be approximated by

$$H_I = -\left[\phi_3 \sin(\pi f_e) - \frac{1}{4}\phi_3^2 \cos(\pi f_e)\right]E_J \cos \phi, \quad (20)$$

with

$$\phi_3 = \left[\frac{4E_c}{\alpha(1 + \beta)E_J} \right]^{1/4} (a + a^\dagger), \quad (21)$$

where a (a^\dagger) is the operator for annihilating (creating) a boson. Because α and β are large for a large-area left JJ, it is clear that when $f_e \neq 0$, H_I is dominated by a weak one-boson process, while a much weaker two-boson process is involved in H_I for $f_e = 0$.

III. ENERGY SPECTRUM

Below we show the hybridizing effects of the left JJ on the energy spectrum of the qubit in the charge-flux regime with $E_J = E_c$. The energy levels for $f_e = 0$ and $n_g = 0.5$ are given in Figs. 1(b) and 1(c), where a large left JJ with $\alpha = \beta = 20$ is chosen. In contrast to the energy levels of the CPB qubit [cf. Fig. 1(d)], there exist additional levels due to the left JJ. However, because the left JJ is now large (i.e., $E_{J3} = 20E_J$), the interaction between this JJ and the CPB qubit is small. Therefore, the energy levels of the CPB qubit are slightly modified by these additional levels, especially for the two lowest levels used for the qubit.

Figures 2(a) and 2(b) display the energy levels for $f_e = 0$ and $n_g = 0.5$ and a much smaller E_{J3} , since now $\alpha = 3$. The levels of the left JJ now hybridize with those above the two lowest levels, but the two lowest levels are still barely modified [comparing Fig. 2(a) with Fig. 1(d)]. This means that, as far as the two lowest states are concerned, the left JJ with $\alpha = 3$ can still be regarded as a large JJ. When the left JJ becomes even smaller (e.g., $\alpha = 0.3$), H_I becomes larger and the energy

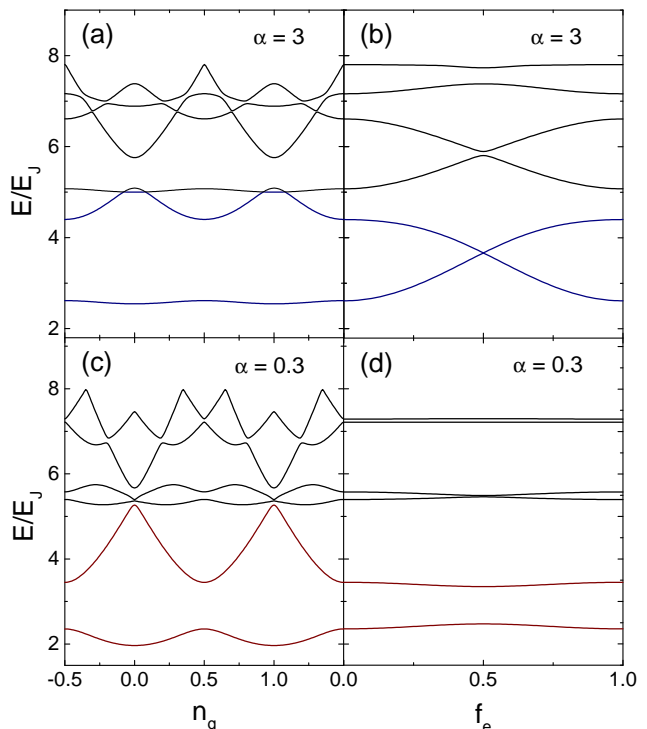


FIG. 2: (Color online) Energy levels of the charge-flux qubit versus n_g at $f_e = 0$ for (a) $\alpha = 3$ and (c) 0.3, and versus f_e at $n_g = 0.5$ for (b) $\alpha = 3$ and (d) 0.3.

levels of both the left JJ and the CPB qubit become heavily hybridized [see Figs. 2(c) and 2(d)]; one can see that the energy levels in Fig. 2(c) look different from those in Fig. 1(b), but the two lowest levels can also be used for a qubit.

IV. STATE COHERENCE AND QUBIT OPTIMIZATION

Realistic qubit circuits will experience fluctuations from both charge and magnetic flux. These noises will affect the coherence of the qubit states in the subspace with basis states $|0\rangle$ and $|1\rangle$, corresponding to the two lowest levels. To characterize the qubit-state coherence, the relaxation time T_1 and decoherence time T_2 are used:¹⁰

$$\begin{aligned} \frac{1}{T_1} &= 4|\langle 0|A|1\rangle|^2 S(\omega_{01}), \\ \frac{1}{T_2} &= \frac{1}{2T_1} + \frac{1}{T_\varphi}, \end{aligned} \quad (22)$$

with

$$\frac{1}{T_\varphi} = |\langle 0|A|0\rangle - \langle 1|A|1\rangle|^2 S(\omega)|_{\omega \rightarrow 0}. \quad (23)$$

Here A is an operator characterizing the coupling between the qubit and the environment, and $S(\omega)$ is the power spectrum of the noise. Moreover, because there

are other levels above the lowest two, leakages from the qubit-state subspace to these outside levels can occur. Therefore, two additional times.¹⁰

$$\frac{1}{T_{Lk}} = 4 \sum_n |\langle n|A|k\rangle|^2 S(\omega_{kn}),$$

$$k = 0, 1, \quad n = 2, 3, \dots, \quad (24)$$

are needed to characterize the noise-induced transitions from the two lowest levels to the ones above.

These results are based on the boson bath model in which the noise is described by a collection of harmonic oscillators with a spectral distribution. When Eq. (22) is applied to a $1/f$ noise (see, e.g., Ref. 11), the very low frequencies are cut off for the power spectrum $S(\omega)$. This cutoff low-frequency part corresponds to the limit of very slow processes. For instance, for the $1/f$ charge noise, this can correspond to the extremely slow switchings of the trapped charges. If these fluctuating processes are much slower than the decoherence time T_2 of the qubit, they remain approximately static during the quantum operation and yield negligible dephasing.

A. Johnson-Nyquist noises

For Johnson-Nyquist noises, such as the fluctuations from gate voltage and external magnetic flux, the operators A are given, respectively, by

$$A_V = \frac{E_{cp}N - E_l N_3}{\sqrt{E_{cp}^2 + E_l^2}}, \quad (25)$$

and

$$A_\Phi = \cos(\phi) \sin(\pi f_e + \frac{1}{2}\phi_3). \quad (26)$$

The power spectrum is given by

$$S(\omega) \equiv J(\omega) \coth\left(\frac{\hbar\omega}{2k_B T}\right), \quad (27)$$

where $J(\omega)$ is the bath spectral density.

For gate-voltage fluctuations characterized by an impedance $Z(\omega)$, the bath spectral density is

$$J_V(\omega) = \frac{2\pi\xi}{R_Q} \omega \text{Re}[Z(\omega)], \quad (28)$$

where

$$\xi = \left[1 + \frac{1}{(1+2\alpha)^2}\right] \left(\frac{C_g}{C_2}\right)^2, \quad (29)$$

and $R_Q = h/e^2 \approx 25.8 \text{ k}\Omega$ is the quantum resistance. Here we choose $C_g = 0.01C_2$, and consider the typical

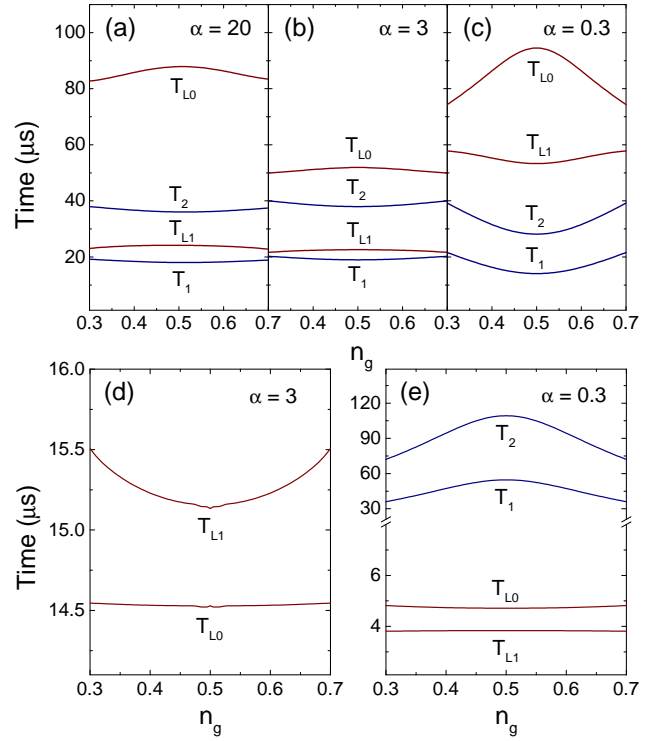


FIG. 3: (Color online) Relaxation (T_1), decoherence (T_2), and leakage (T_{L0} and T_{L1}) times versus n_g at (a) $\alpha = 20$, (b) 3, and (c) 0.3 for gate-voltage noise, and at (d) $\alpha = 3$ and (e) 0.3 for flux noise, where $f_e = 0$. In (d), T_1 and T_2 are not shown because they are 5 orders of magnitude larger than T_{L0} and T_{L1} . Here the temperature is chosen to be $T = 30 \text{ mK}$.

Ohmic case of $Z(\omega) = R_V = 50 \Omega$. The external magnetic flux in the qubit loop is produced by a coil of inductance L and resistance R_L . The bath spectral density of the external magnetic flux fluctuations is

$$J_\Phi(\omega) = \frac{\pi}{2} \left(\frac{R_Q}{R_L}\right) \frac{\eta^2 \omega}{[1 + (\omega L/R_L)^2]}, \quad (30)$$

where

$$\eta = \frac{M I_c}{\Phi_0}, \quad (31)$$

with $I_c = 2\pi E_J/\Phi_0$, and M is the mutual inductance between the qubit loop and the coil. Here we choose $E_J/h = 20 \text{ GHz}$, $R_L = 100 \Omega$, $L = 30 \text{ pH}$, and $M = 5 \text{ pH}$. These parameters correspond to realistic circuits.

Figures 3(a)-3(c) show the four characteristic times at $\alpha = 20, 3$, and 0.3 for the gate-voltage noise. These four times are almost of the same order of magnitude for different sizes of the left JJ; especially T_1 (the minimum of them) and T_2 do not change much. This implies that the gate-voltage noise is mainly determined by the ratio of E_J/E_c and less sensitive to the variation of the left JJ. The observation that T_{L0} and T_{L1} have almost the same order of magnitude as T_1 and T_2 also means that in this case the leakages produce equivalently important

effects on the qubit states as the relaxation and decoherence in the qubit-state subspace. However, for the noise due to external flux fluctuations, the leakages dominate over the relaxation and decoherence [cf. Figs. 3(d) and 3(e)]. Moreover, when the external magnetic flux is around zero, the effects of the external flux noise are sensitive to the variation of the left JJ. For instance, when the left JJ decreases in size to $\alpha = 3$, the leakage times in the flux-noise case are comparable to the relaxation time T_1 in the case of gate-voltage noise [comparing Fig. 3(d) with Figs. 3(a)-3(c)], and the qubit-state leakages become more serious with α decreasing further [see Fig. 3(e)].

The above numerical results for the Johnson-Nyquist noises show that *the decoherence time* $T_2 \gtrsim 30 \mu\text{s}$ or more, *much longer than the experimental value* $T_2 \approx 0.5 \mu\text{s}$ in Ref. 4. This indicates that they could not be the major sources of decoherence in the charge-flux qubit. Instead, because the $1/f$ noise may be the main source of decoherence, we further study its effects on the charge-flux qubit.

B. $1/f$ charge and flux noises

There have been numerous attempts to model $1/f$ noise; including using a collection of independent bistable fluctuators with a given distribution of flipping rates^{12,13} or by interacting two-level classical fluctuators.¹⁴ Alternatively, one can also model it using a boson bath with a $1/f$ spectral density.¹⁵ For the charge-flux qubit considered here, there can be two independent $1/f$ charge noises related with the background charge fluctuations of the CPB and the left JJ; the leakage rates $1/T_{Lk}$ as well as the relaxation and decoherence rates $1/T_i$ ($i = 1, 2$) are the sum of their respective contributions. These two charge noises can be characterized by the power spectra

$$\begin{aligned} S_{q,cp}(\omega) &= \left(\frac{2E_{cp}}{\hbar e} \right)^2 \frac{\alpha_q}{\omega}, \\ S_{q,l}(\omega) &= \left(\frac{2E_l}{\hbar e} \right)^2 \frac{\alpha_q}{\omega}, \end{aligned} \quad (32)$$

with the corresponding operators A being

$$\begin{aligned} A_{q,cp} &= -i \frac{\partial}{\partial \phi}, \\ A_{q,l} &= -i \frac{\partial}{\partial \phi_3}. \end{aligned} \quad (33)$$

Here, for simplicity, $\alpha = \beta$, and α_q is chosen here to be the same for these two charge noises. In Ref. 4, $\beta > \alpha$ because a current source is connected in parallel to the left JJ; this decreases $E_l \equiv 4E_{cp}/(1 + \beta)$, and the dephasing due to the $1/f$ charge noise of the left JJ is weaker than that of $\beta = \alpha$. Also, we can define a power spectrum for the $1/f$ flux noise:

$$S_{\Phi}(\omega) = \left(\frac{2\pi E_J}{\hbar \Phi_0} \right)^2 \frac{\alpha_{\Phi}}{\omega}. \quad (34)$$

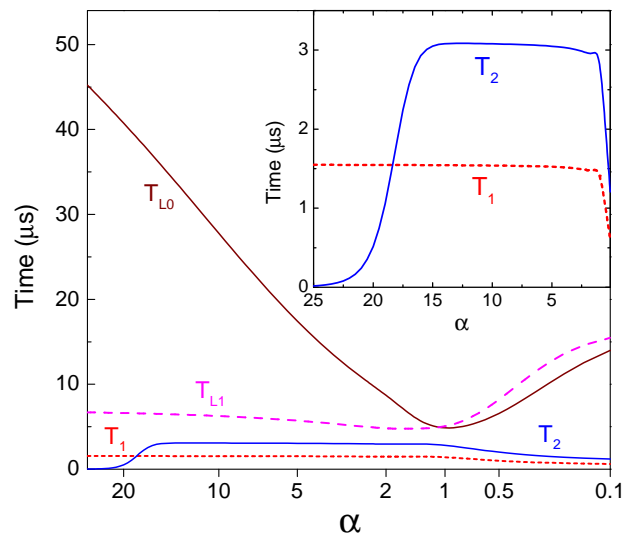


FIG. 4: (Color online) Relaxation (T_1), decoherence (T_2), and leakage (T_{L0} and T_{L1}) times versus α at $(n_g, f_e) = (0.5, 0)$ in the presence of $1/f$ charge noise, where $E_J/h = 20$ GHz is chosen. Inset: T_1 and T_2 are replotted with α scaled linearly.

The corresponding operator A is

$$A_{\Phi} = \cos(\phi) \sin(\pi f_e + \frac{1}{2} \phi_3), \quad (35)$$

which is identical to Eq. (26).

Figure 4 shows the four characteristic times at the degeneracy point $(n_g, f_e) = (0.5, 0)$ in the presence of the $1/f$ charge noise. We choose $\alpha_q = (0.7 \times 10^{-3} e)^2$ for the power spectrum, which is very close to the value used for fitting the experimental data of the $1/f$ noise in the charge qubit.¹⁶ The cutoff frequency is chosen to be $\omega_c/2\pi = 60$ Hz, corresponding to a time scale $\sim 2 \times 10^4 \mu\text{s}$, much slower than the experimentally measured decoherence time $0.5 \mu\text{s}$ of the charge-flux qubit.⁴ To compare the effects of both charge and flux noises, we take the same cutoff frequency for the $1/f$ flux noise. Moreover, we use $\alpha_{\Phi} = 3 \times 10^{-12} \Phi_0^2$ for the flux-noise power spectrum, which is the experimentally determined value of the flux qubit.¹¹ In Fig. 4, the obtained leakage times T_{L0} and T_{L1} are longer than T_1 and T_2 . This means that the leakage is not significant for the $1/f$ charge noise, even though the two lowest levels for the qubit are not very separated from the higher levels (cf. Figs.1 and 2).

We also calculated the four characteristic times for the $1/f$ flux noise at $(n_g, f_e) = (0.5, 0)$ and found that they are much longer than the corresponding characteristic times for the $1/f$ charge noise. Thus, we conclude that the $1/f$ flux noise plays the least dominant role at the degeneracy point for the qubit in the charge-flux regime with $E_J = E_c$. Moreover, for both $1/f$ charge and flux noises, we found that, in the vicinity of the degeneracy point $(n_g, f_e) = (0.5, 0)$, T_1 , T_{L0} , and T_{L1} depend weakly on n_g and f_e . The decoherence time T_2 also depends weakly on f_e (n_g) for the $1/f$ charge (flux) noise, but very

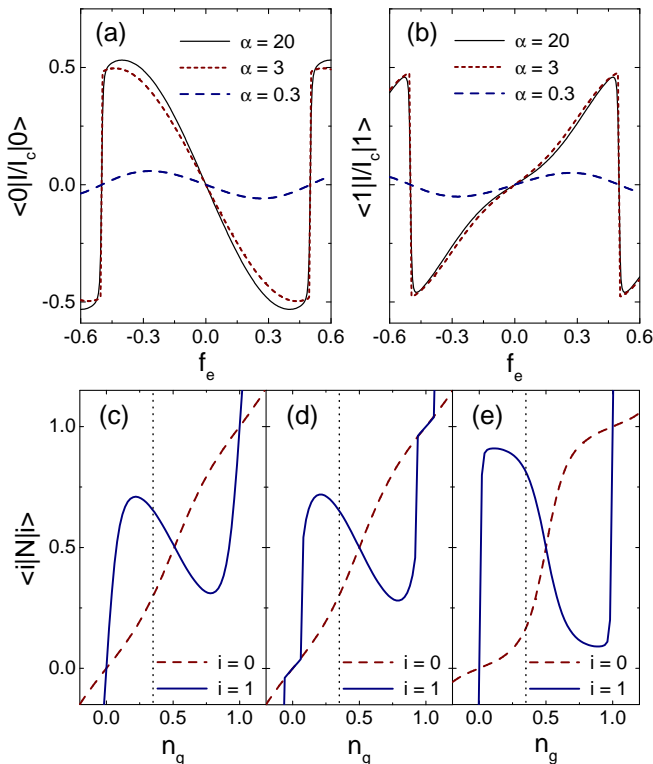


FIG. 5: (Color online) Circulating currents in the qubit loop versus f_e for eigenstates $|i\rangle$, (a) $i = 0$ and (b) 1, where $n_g = 0.5$. The number of Cooper pairs on the island versus n_g at eigenstates $|i\rangle$ for (c) $\alpha = 20$, (d) 3, and (e) 0.3.

strongly on n_g (f_e); slightly away from the degeneracy point along n_g (f_e), the decoherence time T_2 decreases several orders of magnitudes.

For clarity, the relaxation and decoherence times T_1 and T_2 are replotted in the inset of Fig. 4 for the $1/f$ charge noise. At $\alpha = 20$, $T_2 \approx 0.5 \mu\text{s}$, and $T_1 \approx 1.6 \mu\text{s}$. Note that this agrees with the experimental results⁴ of the charge-flux qubit with a large left JJ. Also, it can be seen that the relaxation time remains at $T_1 \sim 1.5 \mu\text{s}$ until $\alpha \sim 1.3$, while the decoherence time T_2 first increases with decreasing α , then remains at $T_2 \sim 3 \mu\text{s}$ (the longest decoherence time) when $1.3 \lesssim \alpha \lesssim 16$, and finally falls down for $\alpha \lesssim 1.3$. Therefore, one can optimize the charge-flux qubit in the region $1.3 \lesssim \alpha \lesssim 16$, so that the qubit has the lowest decoherence.

V. EFFICIENT QUANTUM MEASUREMENT

Finally, we focus on how to raise the readout efficiency. Figures 5(a) and 5(b) display the circulating current I in the qubit loop at eigenstates $|0\rangle$ and $|1\rangle$. It is clear that the currents $\langle i|I/I_c|i\rangle$, for $\alpha = 20$ and 3, are close to each other. This further indicates that the left JJ with $\alpha = 3$ still behaves like a large JJ barely affecting the CPB qubit. Here we consider the readout scheme

in Ref. 4, where a current pulse is applied to the qubit circuit via a current source connected in parallel with the left JJ. This gives rise to an effective capacitance C_3 with a larger value of β . Thus, the effect of the left JJ on the CPB qubit is further weakened because the interaction Hamiltonian H_I decreases when increasing β .

For a single left JJ without the right CPB in Fig. 1(a), when biased by a current pulse, it switches at

$$I_{\text{sw}}(\alpha) \sim I_{c3}(\alpha), \quad (36)$$

with a narrow switching-probability distribution, from the zero-voltage state to the dissipative nonzero-voltage state. Here $I_{c3}(\alpha) = \alpha I_c$ is the critical current of the left JJ. However, when the current pulse is biased to the qubit circuit, i.e., the left JJ plus the right CPB [see Fig.1(a)], the left JJ switches at

$$I_{\text{sw}}^{\text{(qubit)}} = I_{\text{sw}}(\alpha) + \langle i|I|i\rangle \quad (37)$$

with probabilities $p_i(s_i)$ ($i = 0, 1$) which depend on (see, e.g., Ref. 17)

$$s_i = \frac{I_{\text{sw}} + \langle i|I|i\rangle}{I_{c3}}. \quad (38)$$

In Ref. 4, $\alpha = 20$, and the switching-probability difference is found to be as small as

$$|p_0 - p_1| \sim 0.1 \quad (39)$$

because

$$|s_0 - s_1| = \frac{|\langle 0|I/I_c|0\rangle - \langle 1|I/I_c|1\rangle|}{\alpha} \quad (40)$$

is small for $\alpha = 20$. However, when the left JJ becomes smaller, to $\alpha = 3$,

$$|\langle 0|I/I_c|0\rangle - \langle 1|I/I_c|1\rangle|$$

remains nearly unchanged, but $|s_0 - s_1|$ is enlarged about seven times. This greatly increases $|p_0 - p_1|$ and thus efficiently discriminates the states $|0\rangle$ and $|1\rangle$.

In Figs. 5(c)-5(e), we show the number of Cooper pairs on the island, $\langle i|N|i\rangle$, at eigenstates $|i\rangle$, $i = 0, 1$. For a given i , $\langle i|N|i\rangle$ at $\alpha = 20$ and 3 are similar to each other but much different from that at $\alpha = 0.3$. For instance, when $n_g = 0.34$ (indicated by a vertical black dotted line), the number difference

$$\Delta N \equiv |\langle 0|N|0\rangle - \langle 1|N|1\rangle|$$

is $\Delta N \sim 0.37$ for both $\alpha = 20$ and 3, but increases to $\Delta N \sim 0.67$ when $\alpha = 0.3$. Therefore, the readout efficiency for discriminating the states $|0\rangle$ and $|1\rangle$ can be much increased at $\alpha = 0.3$, when a single-electron transistor¹⁸ is capacitively connected to the island and used for measuring the quantum states. Also, one can effectively couple two CPB qubits with $\alpha = 0.3$ by taking advantage of the charge degree of freedom, such as connecting the islands in the two qubits via a mutual capacitance (see, e.g., Ref. 19). This capacitive coupling can be used to reduce decoherence in a logical qubit composed of two CPB qubits.²⁰

VI. CONCLUSION

In conclusion, we have studied a hybridized charge-flux qubit in which an additional JJ is added into the SQUID loop of the CPB. The goal is to find a low-decoherence superconducting qubit. This is one of the most important open issues since quantum computing is possible only if a qubit with long enough decoherence time becomes available.

Currently, $1/f$ noise is believed to be the main source of decoherence in a superconducting qubit. Here we consider the effects of both charge and flux $1/f$ noises on the hybridized charge-flux qubit. We find that the qubit is optimized in the region $1.3 \lesssim \alpha \lesssim 16$, so that the qubit has the lowest decoherence. These results indicate how to optimize a qubit that is expected to have a longer decoherence time. Moreover, we find that the readout scheme via measuring currents, like that in Ref. 4, can also be optimized, so that the efficiency for discriminating qubit states is much increased. Furthermore, we show that an efficient readout scheme by measuring charges can be achieved as well.

Note that our studies on the $1/f$ noise use the harmonic bath model with a $1/\omega$ spectral density. This is valid when the $1/f$ noise is not dominated by a few fluctuators strongly coupled to the qubit. Here, due to the lack of available data for a charge-flux qubit, the numerical values of α_q and α_Φ in the power spectra of $1/f$ charge and flux noises are chosen from the experimental data of the charge and flux qubits. Also, for simplicity, the same frequency cutoff is used for both charge and flux $1/f$ noises. In some cases, this might considerably deviate from the realistic samples. Thus, more experimental data are needed for giving a quantitative comparison with realistic samples.

Acknowledgments

We thank Y. Nakamura, Yu. Pashkin, O. Astafiev, T. Yamamoto, S.Y. Han, and Y.X. Liu for discussions. This work was supported in part by the National Security Agency (NSA) and Advanced Research and Development Activity (ARDA) under Air Force Office of Research (AFOSR) contract number F49620-02-1-0334, and by the National Science Foundation grant No. EIA-0130383. J.Q.Y. was also supported by the National Natural Science Foundation of China grant Nos. 10474013 and 10534060.

-
- ¹ Y. Nakamura, Yu. A. Pashkin, and J.S. Tsai, *Nature* (London) **398**, 786 (1999); Yu. A. Pashkin, T. Yamamoto, O. Astafiev, Y. Nakamura, and J.S. Tsai, *ibid.* **421**, 823 (2003).
- ² Y. Yu, S.Y. Han, X. Chu, S.I. Chu, and Z. Wang, *Science* **296**, 889 (2002); J.M. Martinis, S. Nam, J. Aumentado, and C. Urbina, *Phys. Rev. Lett.* **89**, 117901 (2002).
- ³ I. Chiorescu, Y. Nakamura, C.J.P.M. Harmans, and J.E. Mooij, *Science* **299**, 1869 (2003).
- ⁴ D. Vion, A. Aassime, A. Cottet, P. Joyez, H. Pothier, C. Urbina, D. Esteve, and M.H. Devoret, *Science* **296**, 886 (2002).
- ⁵ J.Q. You and F. Nori, *Phys. Rev. B* **68**, 064509 (2003); J.Q. You, J.S. Tsai, and F. Nori, *ibid.* **68**, 024510 (2003); Y.X. Liu, L.F. Wei, and F. Nori, *Europhys. Lett.* **67**, 941 (2004).
- ⁶ A. Blais, R.S. Huang, A. Wallraff, S.M. Girvin, and R.J. Schoelkopf, *Phys. Rev. A* **69**, 062320 (2004); A. Wallraff, D. I. Schuster, A. Blais, L. Frunzio, R.S. Huang, J. Majer, S. Kumar, S. M. Girvin, and R. J. Schoelkopf, *Nature* (London) **431**, 162 (2004).
- ⁷ I. Chiorescu, P. Bertet, K. Semba, Y. Nakamura, C.J.P.M. Harmans, and J.E. Mooij, *Nature* (London) **431**, 159 (2004).
- ⁸ T.P. Orlando, J.E. Mooij, L. Tian, C.H. van der Wal, L.S. Levitov, S. Lloyd, and J.J. Mazo, *Phys. Rev. B* **60**, 15398 (1999).
- ⁹ J.Q. You, Y. Nakamura, and F. Nori, *Phys. Rev. B* **71**, 024532 (2005); Y.X. Liu, J.Q. You, L.F. Wei, C.P. Sun, and F. Nori, *Phys. Rev. Lett.* **95**, 087001 (2005).
- ¹⁰ G. Burkard, R.H. Koch, and D.P. DiVincenzo, *Phys. Rev. B* **69**, 064503 (2004).
- ¹¹ P. Bertet, I. Chiorescu, G. Burkard, K. Semba, C.J.P.M. Harmans, D.P. DiVincenzo, and J.E. Mooij, *Phys. Rev. Lett.* **95**, 257002 (2005).
- ¹² E. Paladino, L. Faoro, G. Falci, and R. Fazio, *Phys. Rev. Lett.* **88**, 228304 (2002).
- ¹³ Yu.M. Galperin, B.L. Altshuler, and D.V. Shantsev, *cond-mat/0312490*; L. Faoro, J. Bergli, B.L. Altshuler, and Y.M. Galperin, *Phys. Rev. Lett.* **95**, 046805 (2005).
- ¹⁴ A.K. Nguyen and S.M. Girvin, *Phys. Rev. Lett.* **87**, 127205 (2001).
- ¹⁵ Yu. Makhlin and A. Shnirman, *JETP Lett.* **78**, 497 (2003); *Phys. Rev. Lett.* **92**, 178301 (2004).
- ¹⁶ Y. Nakamura, Yu.A. Pashkin, T. Yamamoto, and J.S. Tsai, *Phys. Rev. Lett.* **88**, 047901 (2002).
- ¹⁷ A. Cottet, D. Vion, A. Aassime, P. Joyez, D. Esteve, and M.H. Devoret, *Physica C* **367**, 197 (2002).
- ¹⁸ M.H. Devoret and R.J. Schoelkopf, *Nature* (London) **406**, 1039 (2000).
- ¹⁹ M.H.S. Amin, *Phys. Rev. B* **71**, 024504 (2005).
- ²⁰ J.Q. You, X. Hu, and F. Nori, *Phys. Rev. B* **72**, 144529 (2005).